



# Component test for the assessment of delayed hydrogen-assisted cracking in thick-walled SAW joints for offshore applications

Michael Rhode<sup>1,2</sup> · Arne Kromm<sup>1</sup> · Tobias Mente<sup>1</sup> · Daniel Brackrock<sup>1</sup> · Denis Czeskleba<sup>1</sup> · Thomas Kannengiesser<sup>1,2</sup>

Received: 25 September 2023 / Accepted: 5 December 2023  
© The Author(s) 2023

## Abstract

Offshore wind turbines continuously increase in size and weight and demand adequate offshore foundations concepts like monopiles, tripods, or jackets. These components are typically constructed using submerged arc welding (SAW) with high-strength thick steel plates like the S420ML. During welding, the occurrence of delayed hydrogen-assisted cracking (HAC) must be anticipated. HAC is a critical combination of the local hydrogen concentration within a susceptible microstructure under certain mechanical load, i.e., the occurring (welding) residual stresses. The welding sequence of the thick-walled plates complicates the residual stress distribution due to the necessary repeated thermal cycling, i.e., welding seam/layer deposition to fill the joint. For that purpose, SAW with two-wire-technique was used to weld a specially designed and prototype-like mock-up of a real component with a thickness of 50 mm, filled with over 20 passes and a seam length of 1000 mm. Additional welded stiffeners simulated the effect of a high restraint, to achieve critical HAC conditions. The necessity of a minimum waiting time (MWT) before the NDT can be conducted (to exclude HAC) was critically verified by the application of ultrasonic testing of the welded joint at different time-steps of the NDT of up to 48 h after the completion welding. The residual stresses were determined by a robot XRD goniometer. Tensile residual stresses up to the yield limit are found both in the weld metal and in the heat-affected zone. Numerical modeling allowed the qualitative estimation of the hydrogen diffusion in the weld. No noticeable HAC occurrence was identified and confirms the high cracking resistance of the investigated material. Finally, the applicability of the MWT concept should be critically discussed.

**Keywords** Hydrogen · Cold cracking · Submerged arc welding · Offshore · Thick plates

## 1 Introduction

For the offshore wind turbine (OWT) foundations, mostly high-strength steels are used like the thermo-mechanically rolled steel S420ML. The predominant welding process used is the submerged arc welding (SAW) due to its high efficiency and suitability for thick plates in offshore environments. The underlying standards define a minimum waiting time (MWT) of up to 24 h ( $R_{eH} < 460$  MPa) [1] before NDT is allowed [2], to exclude delayed hydrogen-assisted

cracking (HAC). Possible sources of hydrogen are, e.g., moisture of welding flux or condensates on the welding plate surface. The time-delayed HAC is typically described as the result of a critical combination of a hydrogen concentration within a susceptible microstructure under sufficient mechanical load [3]. In that connection, the residual stresses (RS) caused by welding fabrication are a major concern for HAC in combination with the absorbed hydrogen. Welded joints of thick steel plates imply a very stiff construction. That means the welds are subjected to a severe shrinkage and angular distortion restraint intensity during cooling, which generates additional high reaction forces and corresponding component-related RS.

The scientific background and challenge are the transferability of such real-world service mechanical load scenarios to laboratory conditions and vice versa [4, 5]. In most cases, tests on original components are too expensive or simply not feasible. For example, the widely applied monopiles can reach a diameter of 8 m and a length of 80 m encompassing

---

Recommended for publication by Commission II - Arc Welding and Filler Metals

---

✉ Michael Rhode  
michael.rhode@bam.de

<sup>1</sup> Bundesanstalt für Materialforschung und -prüfung (BAM), Berlin, Germany

<sup>2</sup> Otto-von-Guericke-University, Magdeburg, Germany

a total weight of > 100 metric tons [6]. For that purpose, scaled weld mock-ups are used to simulate the high mechanical stiffness found in real large components on a laboratory scale. Also, the comparison with numerical models requires a reduction in the size of the original component to minimize the modeling effort. For this purpose, the component-like models are designed, which usually only simulate the critical areas of a welded component.

Especially in the safety-critical area of nuclear reactors, mock-ups often serve to reproduce the RS that form in the thick plate welds causing weld joint cracking phenomena. In addition to austenitic steel [7], Zr alloys [8] and dissimilar joints were studied [5, 9, 10]. Francis et al. [4] used mock-ups of several length scales to map different effects, such as RS or distortion and heat flow. Kim et al. [11] studied the effect of the size of a mock-up compared to the original component. A nozzle from a nuclear power plant joint was gradually reduced in size from the original scale to 25 % of its size. It was found that RS were significantly affected by the size of the mock-up. The influence of weld pass, i.e., the weld bead, size was also investigated. Using the original bead size resulted in the highest RS. Mock-ups are not only focused on RS. Kangas et al. [12] show that the degree of restraint can also influence the toughness of welded joints. Thus, the formation of certain precipitates can be accelerated by high reaction forces. Similar phenomena were observed by the authors during welding and heat treatment of a CrMoV steel [13]. Especially in the field of SAW of thick plates, an integrity evaluation based on mock-ups is useful due to the high stiffnesses and unique heat conduction of real components.

For that reason, a component-like test geometry (so-called mock-up) was created to simulate rigid structures of realistic large-scale components. The occurring welding RS were determined by X-ray diffraction (XRD). Ultrasonic NDT was performed in accordance with the MWT up to 48 h to identify points of interests (POI) in terms of possible welding defects, especially in terms of pronounced cracks. At the respective POIs, a metallographic inspection was conducted. Supporting numerical simulation of the hydrogen diffusion was conducted. Finally, the combination of the residual stresses and simulated hydrogen concentration allows the estimation of critical conditions for HAC.

## 2 Materials and methods

### 2.1 Investigated materials, welding, and geometry

The following sub-sections present details of the materials, the weld joint geometry, the SAW parameters and the initial hydrogen concentration.

#### 2.1.1 Materials

The investigated base material (BM) was a 50 mm thick plate of the offshore steel grade S420ML+Z35. The welding plates had a width of 250 mm and a length of 1000 mm. For the submerged arc welding (SAW), the welding wire OE-SD3 with 4 mm diameter and the fully basic agglomerated welding flux (OP 121 TT, both from Oerlikon Welding) combination was used. The welding wire corresponds to an EH12K (in accordance with AWS A5.17 [14]) or S3Si (in accordance with DIN EN ISO 14171 [15]). The welding flux is also classified in DIN EN ISO 14171. Table 1 shows the chemical composition of the BM and the weld metal (WM) in the deposited condition; both materials were analyzed by optical emission spectroscopy (OES). The P+S content was < 0.01 wt% for both BM and WM. The chemical composition of the welding flux is shown in Table 2 (in accordance with the manufacturer specifications, shown in reference [16]).

#### 2.1.2 Welding parameters and mock-up geometry

Two ARISTO 1000 AC/DC welding power sources (ESAB, Sweden) were used in combination with the welding head, mounted on a three-axis gantry. Fig. 1a shows the mock-up dimensions (as well as the spots used for residual stress measurement as described in Section 2.2.2). The total weld seam length was 1000 mm, and the mock-up had a total weight of approximately 350 kg. Fig. 1b shows the weld joint geometry details (V-groove with 40° opening angle). As shown in Fig. 1c, more than 20 passes for each mock-up were welded using a tandem welding head (with two independent welding wires, as shown in Fig. 1d). The effect of the stiffeners is shown in Fig. 1e. The corresponding restraint intensity of the selected mock-up geometry was numerically simulated with approximately 20 kN/mm\*mm and represents a very stiff construction as shown in reference [17].

The applied SAW parameters (per wire) were 550 A welding current, 32 V arc voltage (both welding wires in AC-mode), and 610 mm/min welding speed. This resulted in a summarized welding heat input of 3.46 kJ/mm (effective voltage and current values used due to AC-mode).

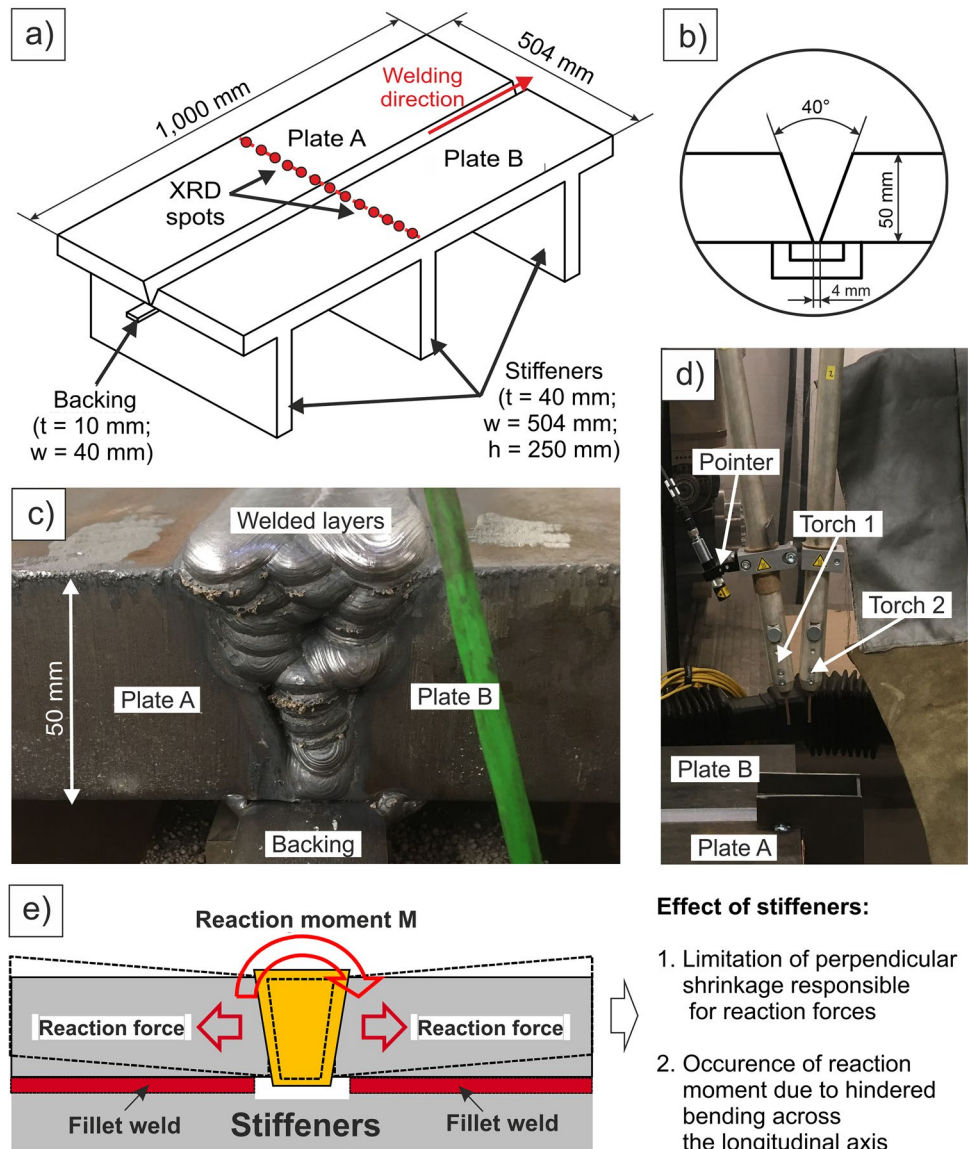
**Table 1** Measured chemical composition of BM and deposited WM (in wt%, Fe-balance)

Grade	C	Mn	Si	Cr	Ni
BM	0.03	1.49	0.35	0.20	0.05
WM	0.05	1.68	0.40	0.05	0.03
Grade	Mo	Al	Cu	Nb	Ti+V
BM	0.01	0.04	0.03	0.019	0.003
WM	0.01	0.02	0.05	0.006	0.007

**Table 2** Nominal composition of weld flux (in wt%) in accordance with manufacturer's specification

MnO	TiO <sub>2</sub>	CaO	CaF <sub>2</sub>	Fe <sub>2</sub> O <sub>3</sub>	SiO <sub>2</sub>	Al <sub>2</sub> O <sub>3</sub>	MgO
2.8	1.5	5.5	22.5	1.0	15.7	21.6	25.0

**Fig. 1** Demonstrator for component-like testing of HAC: **a** mock-up dimensions, **b** weld joint geometry, **c** front-view of final welded component, **d** tandem welding head, and **e** effect of stiffeners on restraint of weld joint



Preheating was not applied in accordance with industrial practice. The interpass temperature was maintained at a maximum of 230 °C. In addition, the  $t_{8/5}$ -cooling time was measured for each single welding pass by insertion of a type K thermocouple in the weld pool behind the welding torch. For that purpose, the thermocouple was inserted through the welding flux within the first 180 mm of the weld seam (connection to measurement equipment and amplifier, visible as green cable in Fig. 1c). The data were used as calibration for the heat source of the numerical simulation (see Fig. 3

and Section 2.3). The interpass temperature was measured in the respective welding pass using a tactile thermocouple.

Prior to the SAW of the mock-up, the three stiffeners (504 mm width, 250 mm height and 40 mm thickness, see Fig. 1a) were attached to the bottom surface of the BM plates with cut-outs along the intended metallic backing. The stiffeners had been welded by gas metal arc welding (GMAW) beneath the welding plates to impede the transverse shrinkage of the joint during welding and the subsequent cooling. As mentioned, the transferability of realistic stiffness conditions

from the field to the lab is very important to ensure realistic testing conditions [4, 5].

### 2.1.3 Variation of initial hydrogen concentration and verification by ISO 3690 samples

Two different initial hydrogen concentrations had been used for the component test. The first condition is the as-received condition of the welding wire and flux combination “HD5,” which means “low hydrogen content” with a hydrogen concentration  $< 5 \text{ ml}/100 \text{ g}$  deposited WM, in accordance with ISO 3690 [18]. For further implications, it is labeled “dry flux” in the following sections. To further provoke hydrogen-assisted cold cracking, the second condition encompassed the use of moist welding flux and is further labeled “wet flux.” For this purpose, the agglomerated welding flux OP 121 TT was exposed to an artificial climate in a climatic chamber for a period of 35 days. The applied exposure conditions were temperature of  $30 \text{ }^\circ\text{C}$  to  $35 \text{ }^\circ\text{C}$  and a relative humidity of 85 % to 98 %. To ensure uniform moistening of the flux, two 25 kg batches were exposed one after the other in the climatic chamber. For each batch, the flux was divided into three tubs, and each tub was mixed at least twice a week. Gravimetric measurement (DIN ISO 11465 [19]) was used to determine the moisture content. After the 35 days “charging” interval, a total moisture content of 3 wt% in the welding flux was achieved. A subsequent 7-day storage at room temperature in laboratory air did not result in any noticeable loss of moisture. Until the intended use for welding, the flux was stored in air-tight containers and the moisture content was determined again before use. No change in the moisture content was measured. Hence, the welding flux was suitable to act as additional hydrogen source during welding.

For that reason, two mock-ups had been manufactured: one with the low hydrogen concentration  $< \text{HD5}$  (industrial practice) and one with a high hydrogen concentration to provoke delayed HAC ( $> \text{HD5}$ ).

### 2.1.4 Hydrogen measurement

To quantify the difference of the hydrogen concentration in the WM, additional ISO 3690 type B samples (in accordance with [18]) were welded (using single wire) with the respective welding parameters presented in the previous section for both dry and wet flux condition. The diffusible hydrogen concentration “HD” was measured by a G8 Galileo (Bruker AXS, Germany) and a coupled quadrupole mass spectrometer (MS) ESD100 (InProcess Instruments, Germany). The analyzer uses the carrier gas hot extraction (CGHE) technique. For that reason, the specimen is heated in an infrared radiation emitting furnace (IR07, part of Galileo G8) placed in a glass tube. The hydrogen in the sample is activated and desorbs from the sample into the carrier gas flow (nitrogen

5.0) and is transferred to the MS for quantitative analysis. The calibration procedure and further details on CGHE were presented elsewhere in the references [20, 21]. Before the hydrogen measurement, the sample was defrosted for 60 s in acetone to ambient temperature and dried in inert nitrogen gas flow for 30 s. The entire transfer procedure from liquid nitrogen to the CGHE analyzer results in a certain hydrogen loss. The authors’ experience shows that typically less than 10 % of the total HD are lost. For comparison to industrial practice, the initial HD was not corrected.

## 2.2 Applied destructive and NDT procedures

The following sub-sections present the experimental details of the applied testing procedures: metallography, residual stress measurement as well as NDT testing of potential cold cracking appearance during the MWT.

### 2.2.1 Metallography, Vickers hardness testing, and SEM investigation

For the metallographic examinations, different cross-sections of the weld seam were extracted from the mock-up after the residual stress measurements. The cuts were made at a sufficient distance from the weld seam. The removal was necessary for the additional radiographic examination (not shown here), as the stiffeners would have hindered the examination. The cross-sections were cut at different positions (POIs) where indications were found during NDT performed beforehand. The cross-sections were manually ground and polished. The microstructure was revealed by etching with 2 % Nital (2 ml nitric acid  $\text{HNO}_3$  dissolved in 100 ml ethanol  $\text{C}_2\text{H}_5\text{OH}$ ) at room temperature for 10 s.

In addition, the macroscopic Vickers hardness HV5 (test load 49.03 N with diamond pyramid indenter) was measured, in accordance with ISO 9015-1 [22]. At representative cross-sections, three hardness measurements were made in (1) the root pass, (2) filler layer with several passes at approximately  $\frac{1}{2}$  of the plate thickness, and (3) at the top/cover layer. For that purpose, a DuraScan 70G hardness tester (EMCO Test Prüfmaschinen GmbH, Germany) was used.

Selected cross-sections were further investigated by scanning electron microscope to identify possible fracture surface morphologies. For that purpose, the respective cross-section was cut by electric discharge machining (EDM) close to the crack tip to avoid mechanical and thermal influence of the crack surrounding. The remaining area was quenched in liquid nitrogen and mechanically opened (broken). Subsequently, the fracture surface was investigated by SEM using a Phenom XL G2 (Thermo Fisher Scientific, Germany) with an acceleration voltage of 15 kV. The corresponding

secondary electrons were detected, and the obtained images interpreted.

### 2.2.2 Residual stress measurement by X-ray diffraction

X-ray diffraction (XRD) was used for residual stress determination. The use of a six-axis robot diffractometer (Xstress Robot from Stresstech Oy, Finland) allowed residual stress analysis without prior sectioning of the mock-up. This made no change or relaxation of the welding RS. The measurement was conducted along the transverse center line in 50 locations of the plate covering the BM, the HAZ, and the WM (red spots in Fig. 1a). Table 3 shows the main measurement and evaluation parameters. The RS were determined by the  $\sin^2\psi$  equation [23–25]. This allows the stress tensor to be calculated assuming that the stress component normal to the surface ( $\sigma_{33}$ ) is zero. The determined RS can also be used to derive the principal normal stresses and their directions.

Due to the relatively time-consuming XRD measurement of such full-scale demonstrators, it was decided to

investigate the mock-up welded with “dry flux” in detail. Due to the nearly identical welding parameters (see Section 2.1), heat input and sample dimensions, the occurring global RS distribution is assumed to be comparable between both mock-ups, although local differences are likely to occur (e.g., annealing of WM by the 2nd last pass by last welding pass).

### 2.2.3 Nondestructive testing by phased-array ultrasonic testing (PAUT)

The two component welds were each visually inspected for surface cracks after completion of welding and subsequent cooling to 35 °C and then monitored for a period of 48 h with respect to cold crack initiation using phased array ultrasonic testing (PAUT). For that purpose, an in-house and custom-made PAUT equipment was used (BAM Division 8.4 “Acoustic and Electromagnetic Methods”). Since for ultrasonic technique (UT), water-based solutions are used for coupling the sound of the probe into the specimen, and due to the sensitivity of the testing technique used to higher temperatures, testing was not started until the specimen was cooled to approximately 35 °C. For that reason, the first test was performed 5 h after welding and was set as reference condition. Additional tests were conducted after 6 h, 12 h, 18 h, 24 h, and 48 h.

For that purpose, the testing was performed from the top surface on both sides of the weld (side A and side B, see Fig. 2a, c in the middle section of the welds excluding the first and last 200 mm of the weld (start and the end of the weld joint with possible SAW process related defects that must be excluded for the HAC assessment) as shown in

**Table 3** Measurement and evaluation parameters for residual stress determination

Radiation	CrK $\alpha$
Lattice plane	{211} $\alpha$
Exposure time	5 s
Collimator	$\phi$ 2 mm
$E^{211}$ ; $\nu^{211}$ (Kroener)	215,000 MPa; 0.242
$\varphi$ -directions	0°; 45°; 90°
$\psi$ -directions	0° $\pm$ 45°; (9 steps each)

**Fig. 2** Setup for PAUT of the welded component: **a** gantry with mounted x, y-transducer, **b** detailed view, and **c** PAUT transducer position for measuring of side A

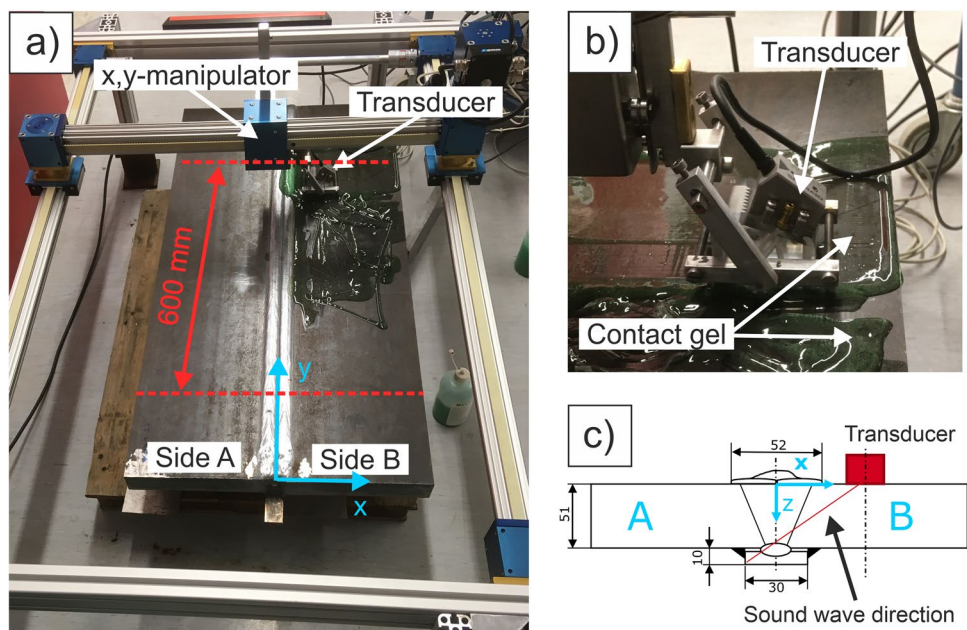


Fig. 2a. The PAUT-sensor was mounted to a  $x$ - $y$ -manipulator allowing to move the sensor along equidistant paths perpendicular to the weld as shown in Fig. 2b. The distance between the paths was set to 2 mm for a certain overlap of the PAUT signals. On each path, the PAUT sensor was moved from the weld to the edge of the mock-up to get information from the whole cross-section of the weld. The use of a phased array allows the acquisition of several single images per measuring point, because the sound angle was changed electronically controlled in the range of  $30^\circ$  to  $65^\circ$  in steps of  $5^\circ$  for each measuring point. The test was performed with a longitudinal wave, as this had a better diffraction behavior at crack tips than the transverse wave.

Computational focusing using the Synthetic Aperture Focusing Technique (SAFT) allows an image with high spatial resolution to be reconstructed and thus more precise statements to be made about possible defects in the weld joint and their changes. Before performing the test, the sensitivity was adjusted on a test wedge with a 2 mm transverse bore and 0.1 mm eroded notch. The depth position of the tip of the eroded notch could be determined to within 0.2 mm deviation after reconstruction using SAFT.

### 2.3 Numerical simulation of hydrogen distribution

The finite element software ANSYS was used to simulate the hydrogen diffusion in the SAW joint. A two-dimensional model of the weld geometry (Fig. 1a) was created using APDL (ANSYS Parametric Design Language). Further details on this procedure and the implementation can be found in the references [26, 27]. The numerical analysis of the hydrogen diffusion dependent on weld thermal cycle should enable identification of crack critical regions in the weld joint by means of peak hydrogen concentration over time during welding and cooling of the sample. The welding process was simulated by moving the isotherm of the three-dimensional molten weld pool through the two-dimensional model, where the temperature of the nodes within the isothermal was above the melting temperature. The validation was carried out by comparing the calculated temperature with the temperature measured in the experiment, see Fig. 3. For that purpose, the individual  $t_{8/5}$ -cooling time per layer was expressed by a mathematical fit (solid line).

The filling of each welding pass was realized via the element birth and death technique in ANSYS. Free convection in air was assumed for all free surfaces of the mock-up. Thermophysical material properties were taken from reference [28] for a similar steel. In the 2nd step, the temperature dependent diffusion coefficients were calculated from the weld thermal cycle and applied to the diffusion analysis [27]. The calculation of the diffusion coefficients is based on the scatter band for diffusion coefficients in low-alloyed steels [29]. Investigations on hydrogen diffusion behavior in weld

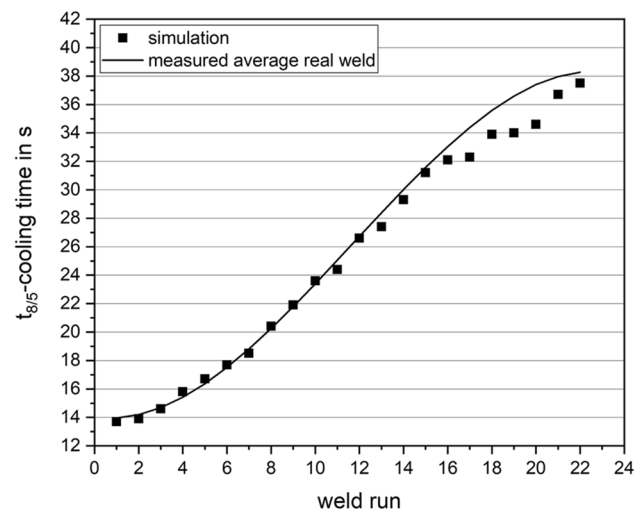


Fig. 3 Calculated  $t_{8/5}$ -time from simulation compared to measured (average)  $t_{8/5}$ -time during welding of pass 1 to 22

metal of a similar SAW steel joints showed that the diffusion coefficients of the weld metal lie in the range of the average curve in the scatter band [30]. Below a temperature of  $50^\circ\text{C}$ , there was a steep drop in the diffusion behavior visible which was also considered for the numerical analysis by applying approximately 10 times lower diffusion coefficients compared to the average diffusion. In the last step, the hydrogen diffusion was simulated by the analogy of Fourier's heat equation and Fick's 2nd law using the thermal module in ANSYS [31]. For each weld pass, the elements reaching the melting temperature were set to a normalized hydrogen concentration of "1" (i.e., 100 %), and free effusion was assumed for all free surfaces of the mock-up. The simulation of the H-diffusion was performed for at least 48-h duration after the weld was cooled down to room temperature. The reason was the simulation of the MWT effect on the hydrogen distribution and identification of areas with increased HAC susceptibility due to a high H-concentration.

## 3 Results and discussion

### 3.1 Initial hydrogen concentration

The measured hydrogen concentration "HD" was 4.6 ml/100 g deposited WM for the "dry flux" and 27.3 ml/100 g deposited WM in case of the "wet flux" (each HD is the mean value of three samples, the corresponding standard deviation was  $< 5\%$ ). From the manufacturing point of view, the measured H-concentration represent a maximum possible hydrogen ingress during welding, which may not be necessarily achieved in the WM. The use of the "dry flux" ensured that the guaranteed HD5-condition

was fulfilled (see removed SAW slag in Fig. 4a). The high moisture content of the “wet flux” provided the source of hydrogen gas, which evaporated from the molten weld metal (WM) and was trapped as molecular hydrogen beneath the glassy slag on top of the deposited WM, as shown in Fig. 4b.

Of course, the “wet flux” represented an extreme scenario, which is unlikely to occur in actual welding fabrication. Nonetheless, this scenario is extremely of interest for very harsh testing conditions, provoking delayed HAC in the welded joints.

### 3.2 Cross-sections and hardness

In Fig. 5a, the cross-section of the welded mock-up with HD of max. 4.6 ml/100 g deposited WM is shown, and in Fig. 5b, the cross-section for the HD of 27.3 ml/100 g deposited WM. It is obvious that the hydrogen concentration did not generally influence the weld joint quality. Defect-free welds (visual inspection of each single pass) with full penetration were achieved for both mock-ups with a total of 22 welding passes (“dry flux”) and 21 respectively (“wet flux”). The ferritic-bainitic microstructure of the BM undergoes

**Fig. 4** Removed slag of SAW ISO 3690 bead-on-plate samples, welded with **a** “dry flux” (HD = 4.6 ml/100 g deposited WM) and **b** “wet flux” (HD = 27.3 ml/100 g deposited WM) with pore formation

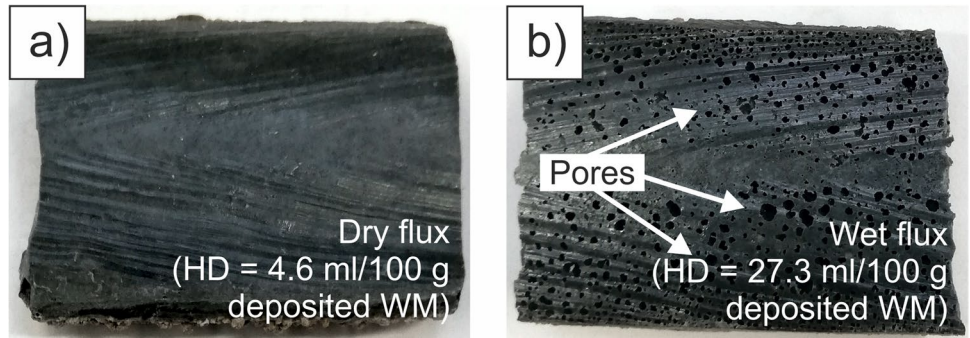
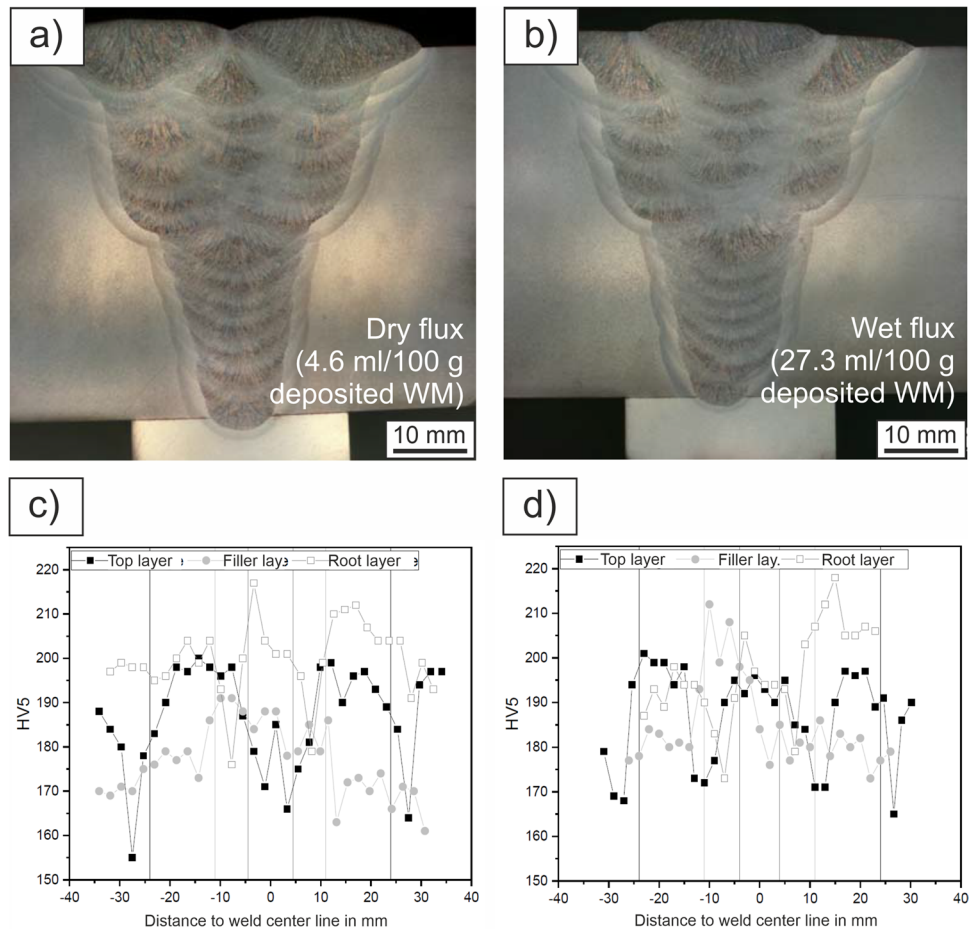


**Fig. 5** Cross-sections of SAW joints: **a** welded with “dry flux” and **b** with “wet flux”; **c, d** corresponding HV5 distributions for root, filler, and top layer



multiple reheating cycles with different peak temperatures, resulting in a complex HAZ subzones structure as well as the deposited WM. The combination of ferrite and bainite indicates a relatively low hardness, for both “dry flux” (Fig. 5c) and “wet flux” (Fig. 5d).

The Vickers hardness ranges between 150 HV5 and 220 HV5. The hardness of the top layer (encompassing two to three passes) is comparable for both mock-ups to the hardness of the filler layers in the centerline region of the weld joint ranging from 180 HV5 to 200 HV5. In opposite, the HV5 in the root layer is slightly higher. This is due to the fast cooling of the first passes, which can be seen in terms of the short  $t_{8/5}$ —cooling time of approximately 14 s (see Fig. 3). In the case of the root passes/layer, the mock-up was still somewhat “cold” due to the missing preheating but warmed up layer by layer (due to the maintained 230 °C interpass temperature) to > 30 s for the final passes. A small decrease/drop of the hardness was regarded for the HAZ-area for both mock-ups. Generally, the relatively low hardness indicates a sufficient ductility of the respective welded HAZ or WM microstructure and vice versa an increased resistance against delayed HAC. From that point of view, the hardness, and the hydrogen ingress (with high or low H-concentration) did not show any obvious interdependency on each other.

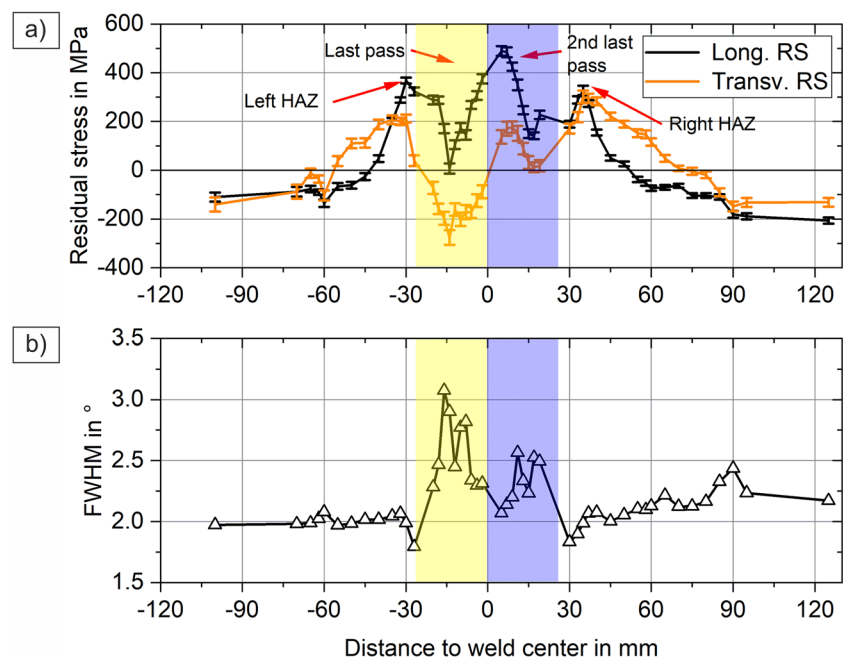
### 3.3 Residual stresses (XRD)

This section presents the determined residual stresses (RS) measured at the positions as indicated in Fig. 1a perpendicular to the welding direction. At each position, both the transverse welding RS (perpendicular to the welding

direction) and the longitudinal RS (in welding direction) were determined. As mentioned in Section 2.1, only the mock-up welded with “dry flux” was investigated in detail. Due to the nearly identical heat input and sample dimension of both mock-ups, the global RS distribution (RS in HAZ and BM) are assumed to be comparable, although local differences are like to occur, e.g., in the WM (due to the different annealing condition by the varying number of passes in the last welding layer).

Fig. 6 shows the obtained RS distribution in the mock-up welded with the “dry flux.” The distribution was characterized by three local maxima for both the longitudinal and transverse RS, as indicated in Fig. 6a. Two of the maxima were found in the respective HAZs close to the fusion line to the left and to the right of the weld centerline. For both the longitudinal and transverse RS (black and orange line respectively), maximum values of + 370 MPa as tensile RS were obtained, which are close to the BM’s experimentally determined yield strength (+ 470 MPa, mean value of three samples, experiments can be found in reference [17]). That means the tensile RS reach nearly 80 % of the BM yield strength. Next to the corresponding left and right HAZ, the transverse RS of the BM are higher (orange line) compared to the longitudinal RS (black line). In addition, the transverse RS (orange line) change to equilibrium compressive RS of about – 200 MPa at a greater distance compared to the longitudinal RS (black line). The reason is to be found in the hindered angular distortion around the longitudinal axis of the weld due to the additional stiffeners at the bottom of the plate (as shown in Fig. 1). The third maximum of the tensile

**Fig. 6** Residual stresses: **a** in longitudinal and transverse direction to the weld, **b** corresponding FWHM





RS was found in the 2nd last pass of the WM (pass width highlighted in Fig. 6a, b by the blue shaded region).

In the longitudinal direction of the weld, the RS here reach the yield strength of the WM of approx. + 460 MPa. In the transverse direction, the maximum level is just about + 200 MPa. The last pass is characterized by a minimum in the residual stress profile. While there is a stress of about 0 MPa in the longitudinal direction, in the transverse direction, the stresses are in compression of about – 250 MPa at the same point. This can have several causes. On the one hand, the high-strength WM exhibits a bainitic-martensitic microstructure, which causes a stress reduction through the occurrence of so-called transformation stresses due to the associated solid phase transformations. On the other hand, a temperature gradient in the thickness direction can lead to a delayed stress buildup (“quenching”) between the surface and the bulk, which also causes the occurrence of minima or maxima. A minimum also appears in the 2nd last pass, but it is less pronounced than that in the last pass. The full-width at half maximum (FWHM) listed in Fig. 6b proves that with the heat input of the last pass, an annealing to the 2nd last pass takes place, which does not lead to a stress reduction. In the transition from the WM to the HAZ, there is a slight decrease in the FWHM, which suggests a softening, also seen for the HV5 measurements (Fig. 5c, d).

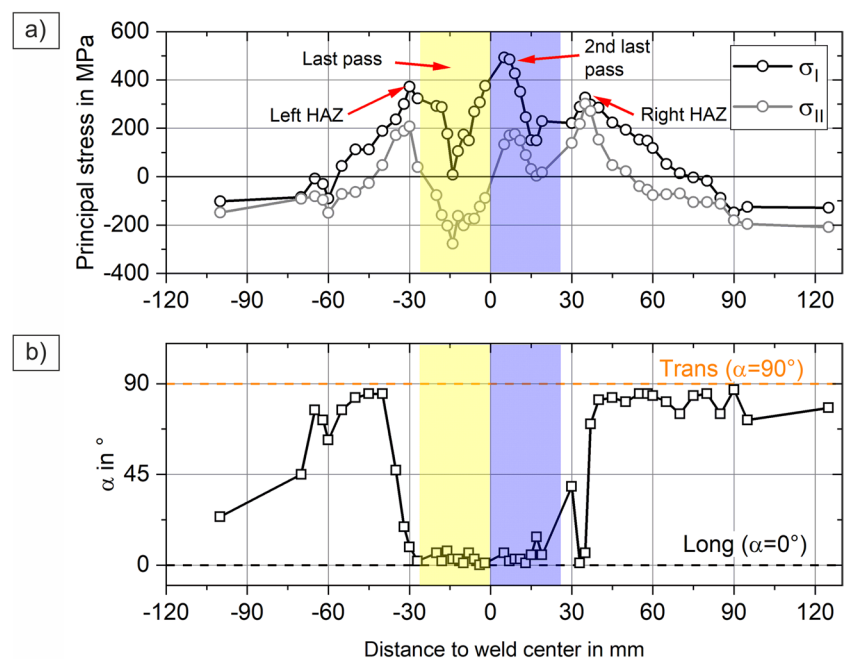
The measurement in several directions  $\varphi$  allowed the calculation of the principal stresses and their directions. Fig. 7 shows the principal stresses. It is obvious that the highest principal stress in both the WM and HAZ corresponds to the longitudinal RS. In the adjacent BM, however, the highest stress is that of the transverse direction. The principal stress

directions are thus dictated by the joint geometry and the associated heat flux, respectively. This is also clear from Fig. 7b, which shows the angle between the direction of the highest principal stress  $\sigma_I$  and the longitudinal direction of the weld. The angle is about  $0^\circ$  in the WM, which corresponds to the longitudinal direction. In the BM, the transverse direction dominates, i.e., the angle is about  $90^\circ$ . In the HAZ, the principal stress direction is between these two values. Due to the surface condition (as-rolled), the principal stress direction in the outer BM exhibits values that are no longer influenced by the thermal effect of welding.

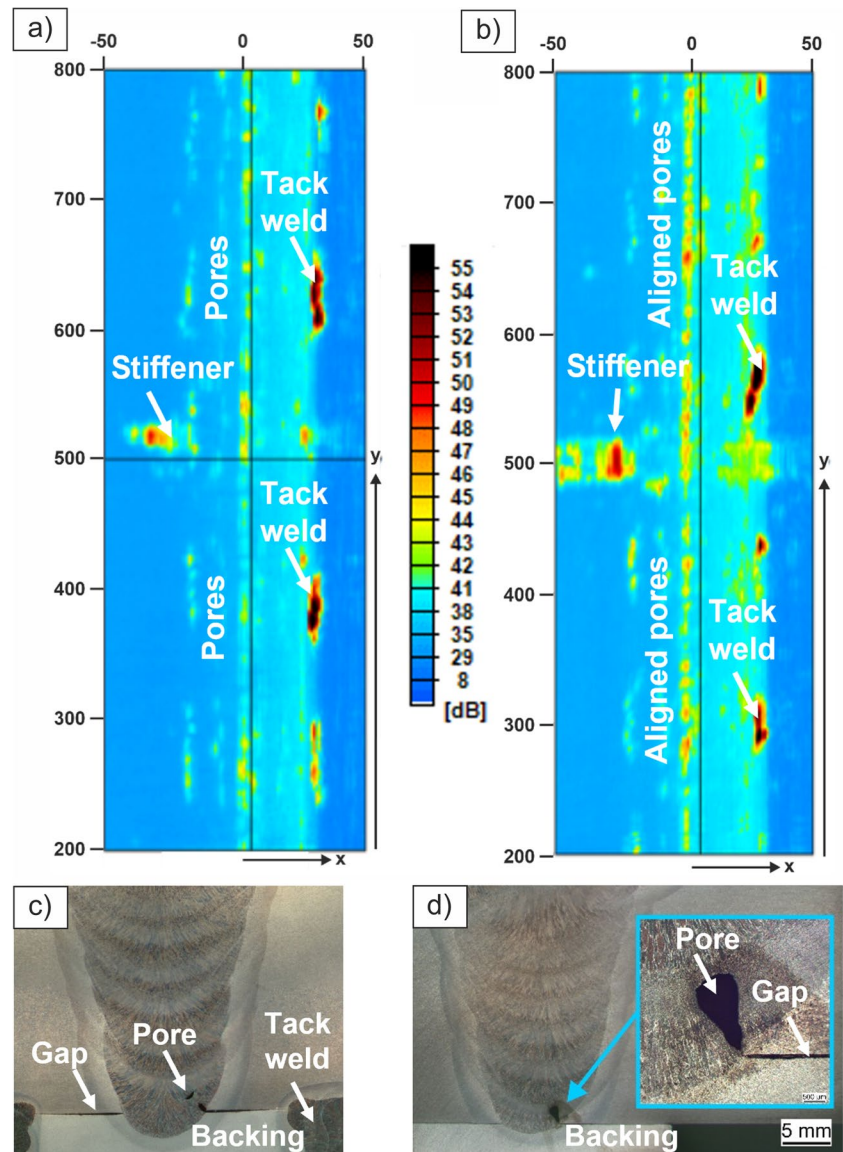
### 3.4 Phased-array ultrasonic testing (PAUT) and metallographic inspection of root pass area

Figure 8a shows the PAUT results (C-scan projection) after the MWT of 48 h for welding condition with “dry flux.” In contrast, Fig. 8b shows the results using the “wet flux,” in other words with a very high hydrogen concentration of 27.3 ml/100 g deposited WM. Both figure parts a and b show the PAUT results for the welding root for  $z = 50$  mm to  $z = 52$  mm (using the coordinate system shown in Fig. 2a, c. Significant reflections (signal amplitude > 50 dB as potential indications for welding defects) were found in both mock-ups. A geometric correlation in the welding direction (y-axis) revealed that identified reflections were the result of (1) the tack welds between the backing and the BM plates and (2) the GMAW fillet welds of the stiffener in the center of the respective mock-up (as schematically shown for the mock-up geometry in Fig. 1e). Nonetheless, the formation of certain welding defects (in terms of pores in the root pass region)

**Fig. 7** Principal stresses: **a**  $\sigma_I$  and  $\sigma_{II}$ , **b** angle “ $\alpha$ ” between longitudinal direction ( $\alpha = 0^\circ$ ) and max. principal stress ( $\sigma_I$ )



**Fig. 8** C-scan projection of PAUT results after maximum MWT of 48 h from a depth of  $z = 50$  mm to 52 mm (root pass area): **a** mock-up welded with dry flux (4.6 ml/100 g deposited WM), **b** mock-up with “wet” flux (27.3 ml/100 g deposited WM) and corresponding cross-sections in **c** and **d**



was found for both mock-ups, independently of the initial hydrogen ingress. This can be seen either in Fig. 8c using “dry flux” resulting in HD = 4.6 ml/100 g (deposited WM) or in Fig. 8d using the “wet flux” with HD = 27.3 ml/100 g (deposited WM). Nonetheless, the pores are tolerable in accordance with DIN EN ISO 5817 [32]. It is reasonable that the pore formation was a result of the air entering through the gap between the backing and the BM plates (backing was only tack-welded).

The hydrogen effect on the defect appearance was characterized by an intensified formation of (aligned) pores along the welding joint was obtained for “wet flux” encompassing the high hydrogen concentration. These pores appeared were significantly smaller compared with those in the root passes. It is reasonable that these pores are hydrogen-induced. Two reasons must be considered for that: (1) the very high

possible diffusible hydrogen concentration of 27.3 ml/100 g (deposited WM) and (2) the relatively short time for hydrogen diffusion during welding. The high hydrogen concentration tends to form pores due to recombination as molecular hydrogen, as indicated by the SAW slag in Fig. 4b. This is additionally supported by the limited diffusion as a consequence of the relatively thick root pass and the subsequent filler passes. In other words, the dissolved hydrogen amount is too high to diffuse out of the root welding pass before the next pass is welded.

### 3.5 Phased-array ultrasonic testing (PAUT) and metallographic inspection of filler passes

Fig. 9 shows C-scan projections of the PAUT results (side A) for diverse filler passes within a depth from  $z = 23$  mm

to  $z = 42$  mm (filler passes) of the mock-up welded with “wet flux” (27.3 ml/100 deposited WM). The C-scans of side B are not presented. The sub-parts of Fig. 9 represent different waiting times after the PAUT was performed with a) after cooling to RT, b) after 6 h, c) after 12 h, d) after 18 h, e) after 24 h, and f) with the maximum waiting time of 48 h. It is noteworthy that no noticeable differences could be identified in the different C-scan projections. This suggests that no delayed hydrogen assisted cracking occurred within this area during the entire 48 h waiting time.

Nonetheless, POIs were identified for different depth positions as shown in Fig. 9. The light red dots at a position of  $y = 470$  mm and  $y = 780$  mm could represent indications for time-dependent occurrence of an imperfection. Especially at the position of  $y = 470$  mm, a more or less considerable indication occurred (as indicated in Fig. 9a). For that reason, a representative metallographic cross-section at this position (despite others along the entire weld seam) was prepared and further characterized. For that reason, Fig. 10 presents the results of a representative cross-section at the position of  $y = 470$  mm. The colored frames in Fig. 10a indicate the detailed analyzed areas for different depth positions in  $z$ -axis.

Fig. 10a shows the already mentioned pores in the weld root pass close to the backing (see Fig. 8). A residual slag

part of the molten welding flux is shown Fig. 10b, c. The dimensions of both mentioned imperfections suggest a quality level B classification in accordance with DIN EN ISO 5817 [32]. Two of the indications found in the WM at  $y = 470$  mm within a depth of  $z = 17$  mm (see Fig. 10d) and at  $z = 42$  mm (see Fig. 10g) turned out as horizontal cracks in the filling layer, surrounded by (micro-) pores. These areas were examined further. For that purpose, the position of interest (encompassing the observed cracking) was extracted from the weld joint. As mentioned in Section 2.2.1, EDM cuts were made before mechanically opening the cracks (after quenching in liquid nitrogen). However, only the crack at  $z = 17$  mm could be opened successfully and examined by SEM. The surface of the opened cracks are depicted in Fig. 10e, f, showing smooth surfaces within the fracture created by the opening process. The fracture morphology shows typical hot cracking features (solidification cracking like rounded and dendritic-like surfaces). For the first impression, it is uncommon to expect hot cracking instead of HAC. Indeed, hot crack formation in presence of high amounts of hydrogen in molten weld pool was reported in reference [33, 34].

At least, despite of the above discussed weld imperfections (small pores and localized hot cracking), no signs of cold crack formation was found even in the mock-up with the high hydrogen concentration of 27.3 ml/100 g deposited

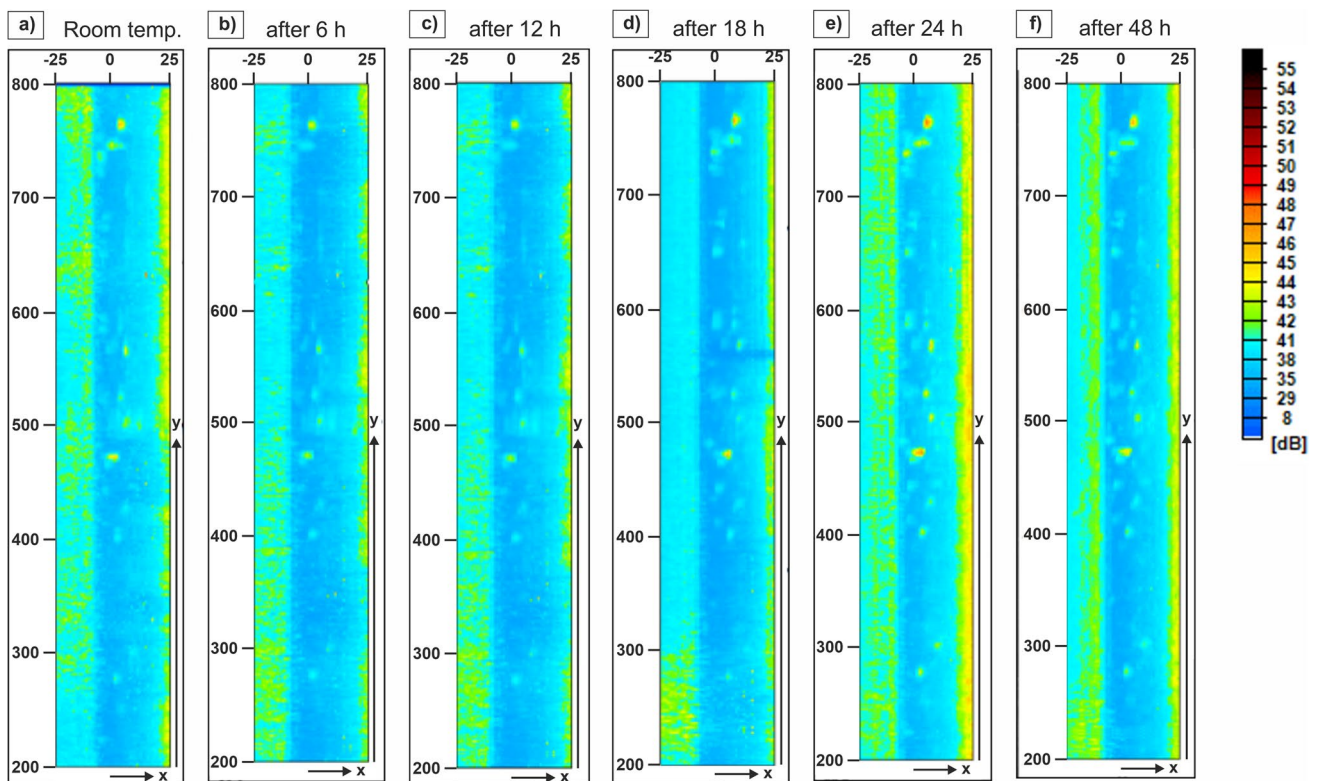
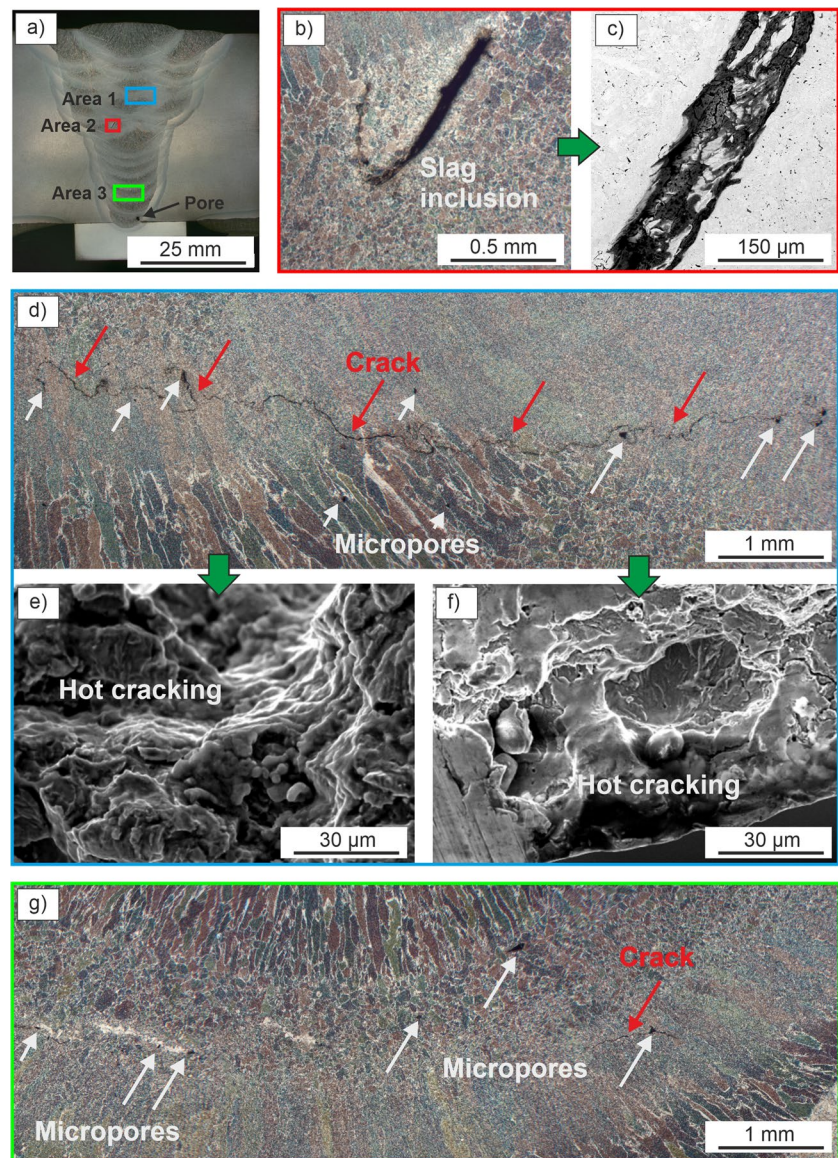


**Fig. 9** C-scan projection of PAUT results of mock-up welded with “wet flux” (27.3 ml/100 g deposited WM); C-scan projection side A from depth of  $z = 23$  mm to 42 mm for all test intervals: **a** reference after cooling to RT (5 h), **b** 6 h, **c** 12 h, **d** 18 h, **e** 24 h, and **f** 48 h

**Fig. 10** Macro-section and details of POIs of the mock-up welded with “wet flux” (27.3 ml/100 g deposited WM) at coordinates of  $y = 470$  mm: **a** overview with areas of interest, **b** Area 1: detail of slag inclusion, **c** SEM-figure, **d** Area 2: detail at depth of  $z = 17$  mm with micropores and horizontal crack, **e**, **f** fracture surface of opened crack with typical hot cracking indications, and **g** Area 3: detail at depth of  $z = 42$  mm with micropores and single crack



WM (“wet flux”). Indeed, the mentioned (hot) cracking was only observed at high H-concentration. From that point of view, the investigated offshore steel grade and its weld joints should have a high resistance against delayed hydrogen-assisted cracking. In addition, the MWT-concept (see Section 1) should be critically assessed. This is consistent with the results on GMA-welded and self-restrained cold cracking tests presented earlier in reference [35].

### 3.6 Numerical simulation

The calculated normalized diffusible hydrogen concentration ( $C/C_0$ ) is shown for welding of the last pass, shown in Fig. 11a and after cooling to RT shown in Fig. 11b. Figure 11c shows the normalized hydrogen concentration in the through thickness direction at this time increment. The metal

weld backing (shown in Fig. 1a) was also considered. As seen from Fig. 11, the hydrogen concentration has reduced to approx. 40 % of the initial concentration after cooling to RT. This is due to the positive effect of the repeated thermal cycles during multi-pass SAW. After cooling to RT, the highest normalized diffusible hydrogen concentration is found in the centerline of the WM at approx. 15 mm beneath the top surface of the weld seam. In the HAZ, a hydrogen concentration of about 36 % of the initial concentration ( $C/C_0 = 0.36$ ) is reached still during the welding process resulting in a maximum concentration of approx. 23 % ( $C/C_0 = 0.23$ ) after cooling to RT. Thus, after welding of the last pass, there is no increase of H-concentration by diffusion in any area of the weld. The choice of adequate hydrogen diffusion coefficients significantly influences the results in terms of the calculated MWT. As we postulated in reference

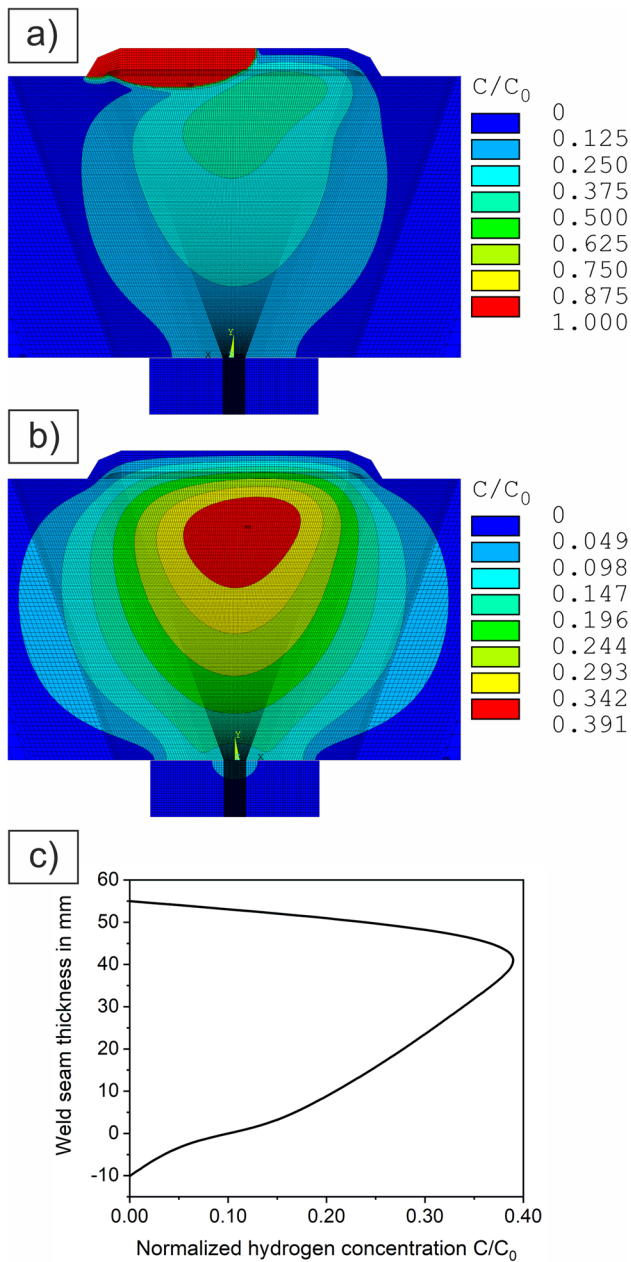


**Fig. 11** Calculated normalized hydrogen concentration  $C/C_0$  in weld seam: **a** welding of last pass, **b** after cooling to RT, and **c** in thickness direction at weld centerline

[30], the MWT effectiveness and necessity just based on a time range are (from that point of view) still questionable and need further clarification.

## 4 Conclusions

Two component-like mock-ups with a weld seam length of 1000 mm and 350 kg were manufactured by the SAW process under consideration of stiffeners to simulate/transfer

mechanical scenarios of practical engineering applications to a laboratory scale. Residual stress measurement was made by XRD as well as further PAUT at different times. Numerical simulations were carried out to assess the hydrogen distribution after welding. The following conclusions can be drawn:

- An experimental sample design was successfully established to simulate very rigid structures as component-like test for delayed hydrogen assisted cracking in offshore steel SAW joints. The reasons are the shrinkage restraint perpendicular to the welding direction and the hindered angular distortion around the longitudinal axis of the weld due to the stiffeners (see Fig. 1e).
- The RS are characterized by maxima in the HAZ (longitudinal and transverse direction) and reach a considerable stress level of 370 MPa, which is approximately 80 % of the (experimentally determined) BM yield strength. The highest, welding tensile RS of 460 MPa are reached in the WM. From that point of view, this area could be critical for a potential crack initiation, although any cold cracking was observed.
- Weld imperfections were successfully localized by PAUT technique. Metallographic cross-sections and the respective POIs revealed imperfections like (micro-) pores. The identified horizontal cracks in the high hydrogen > HD5 (27.3 ml/100 g deposited WM) mock-up had typical hot cracking features, i.e., no delayed cracking by hydrogen.
- The numerical simulation showed that the maximum normalized hydrogen concentration is found in the WM at any time. The hydrogen concentration in the HAZ reaches a maximum of 36 % of the initial concentration still during welding. After cooling to RT, the hydrogen concentration is reduced to 40 % (WM) and 23 % (HAZ).
- Indeed, both mock-ups showed a comparable behavior independently of the hydrogen ingress during welding and the occurring relatively high residual stresses. This means S420ML thick-plate steel and the investigated SAW parameters should ensure a safe welding fabrication without an increased susceptibility for HAC. For that reason, the MWT concept and its necessity should be further assessed and critically discussed.

**Acknowledgements** Sincere thanks is given to Lars Gieseler (Erndtebrücker Eisenwerk GmbH & Co. KG, Germany) for providing the experimental materials and welding consumables. Peter Friedersdorf is thanked for his big support in welding the stiffeners; Marina Marten and Mareike Kirstein are thanked for the metallographic preparation, all with Bundesanstalt für Materialforschung und -prüfung (BAM), Berlin, Germany.

**Funding** Open Access funding enabled and organized by Projekt DEAL. The investigations in this study were partially supported by

the Research Association for Steel Application (FOSTA), grant no. P 1259/32/2017/S 024/10243/17. Open Access funding is enabled and organized by Projekt DEAL.

**Data availability** The raw data is not accessible by the public but can be shared or be made available on demand with private access.

## Declarations

**Competing interests** The authors declare no competing interests.

**Open Access** This article is licensed under a Creative Commons Attribution 4.0 International License, which permits use, sharing, adaptation, distribution and reproduction in any medium or format, as long as you give appropriate credit to the original author(s) and the source, provide a link to the Creative Commons licence, and indicate if changes were made. The images or other third party material in this article are included in the article's Creative Commons licence, unless indicated otherwise in a credit line to the material. If material is not included in the article's Creative Commons licence and your intended use is not permitted by statutory regulation or exceeds the permitted use, you will need to obtain permission directly from the copyright holder. To view a copy of this licence, visit <http://creativecommons.org/licenses/by/4.0/>.

## References

- DIN EN 1090-2 (2018) Execution of steel structures and aluminum structures - part 2: technical requirements for steel structures. German version of EN 1090-2. Beuth-Verlag, Berlin, Germany. <https://doi.org/10.31030/2758614>
- DNVGL-OS-C401 (2015) Fabrication and testing of offshore structures. Classification in accordance with DNV AS (formerly known as DNV GL). Baeum, Norway. Document available via DNV website
- Bailey N, Coe FR, Gooch TG et al (2000) Welding steels without hydrogen cracking, 2nd edn. Woodhead Publishing, Swanston (UK)
- Francis JA, Smith MC, Jeyaganesh B et al (2017) Design and manufacture of industrially representative weld mock-ups for the quantification of residual stresses in a nuclear pressure vessel steel. *Mater Res Proc* 2:581–586. <https://doi.org/10.21741/9781945291173-98>
- Hanninen H, Brederholm A, Sarikka T et al (2014) Rigidity comparison of Alloy 52 narrow-gap weld plate and tubular safe-end mock-up. In: *Structural integrity on Ni-base alloy welds*. VTT Technol 175:220–233
- Negro V, Lopez-Gutierrez JS, Esteban MD et al (2017) Monopiles in offshore wind: preliminary estimate of main dimensions. *Ocean Eng* 133:253–261. <https://doi.org/10.1016/j.oceaneng.2017.02.011>
- Kerr M, Prime MB, Swenson H et al (2013) Residual stress characterization in a dissimilar metal weld nuclear reactor piping system mock-up. *ASME J Press Vessel Technol* 135(4):041205, Paper No. PVT-12-1086. <https://doi.org/10.1115/1.4024446>
- Muransky O, Holden TM, Kirsstein O et al (2013) Evaluation of residual stresses in electron-beam welded Zr<sub>2</sub>5Nb<sub>0.9</sub>Hf Zircaloy flange mock-up of a reflector vessel beam tube flange. *J Nucl Mater* 438(1-3):154–162. <https://doi.org/10.1016/j.jnucmat.2013.02.045>
- Hanninen H, Brederholm A, Sarikka T et al (2014) Alloy 52 narrow-gap and EAC weld mock-ups. In: *Structural integrity on Ni-base alloy welds*. VTT Technol 175:167–173
- Hanninen H, Brederholm A, Sarikka T et al (2014) Residual stress measurements of Alloy 52 narrow-gap weld mock-up. In: *Structural integrity on Ni-base alloy welds*. VTT Technol 175:234–238
- Kim IJ, Jeong JU, Choi JB (2010) A numerical study on mock-up downsizing to predict residual stresses at CRDM welds. In: *Proceedings of the ASME Pressure Vessels and Piping Conference 2010*
- Kangas P, Sorsa I (1983) Effect of multi-run welding on the deformation and fracture toughness of re-strain welded joint. In: Karjalainen P, Rutioaho R (eds) *Proceedings of the 3rd Scandinavian Symposium in Materials Science*. University of Oulu, Oulu, Finland
- Kromm A, Lausch T, Schroepfer D et al (2020) Influence of welding stresses on relief cracking during heat treatment of a creep-resistant 13CrMoV steel - part I: effect of heat control on welding stresses and stress relief cracking. *Weld World* 64(5):807–817. <https://doi.org/10.1007/s40194-020-00875-6>
- AWS A5.17/A5.17M (2019) Specification for carbon steel electrodes and fluxes for submerged arc welding. American Welding Society
- DIN EN ISO 14171 (2016) Welding consumables - solid wire electrodes, tubular cored electrodes and electrode/flux combinations for submerged arc welding of non-alloy and fine grain steels - Classification. German version of EN ISO 14171. Beuth-Verlag, Berlin, Germany. <https://doi.org/10.31030/2403381>
- Oerlikon OP121TT - SAW flux. Manufacturer specification: <https://www.oerlikon-welding.com/de/op-121tt-0>. Accessed 8 August 2023
- Boellinghaus T (2021) Einflüsse auf zeitlich verzögerte Kaltrissbildung und Festlegung der Mindestwartezeit vor der Prüfung der Schweißverbindungen aus Feinkornbaustahl, (in German). Influences on delayed cold cracking and definition of a minimum waiting time before testing). Final report of Project P 1259. Forschungsvereinigung Stahlanwendung e.V. (Research Association for Steel Application), Germany
- DIN EN ISO 3690 (2018) Welding and allied processes - determination of hydrogen content in arc weld metal. German version of EN ISO 3690. Beuth-Verlag, Berlin, Germany. <https://doi.org/10.31030/3002668>
- DIN ISO 11465 (1996) Soil quality - determination of dry matter and water content on a mass basis - gravimetric method. German version of ISO 11465. Beuth-Verlag, Berlin, Germany
- Rhode M, Schaupp T, Muenster C et al (2018) Hydrogen determination in welded specimens by carrier gas hot extraction - a review on the main parameters and their effects on hydrogen measurement. *Weld World* 63:511–526. <https://doi.org/10.1007/s40194-018-0664-9>
- Salmi S, Rhode M, Juettner S et al (2015) Hydrogen determination in 22MnB5 Steel grade by use of carrier gas hot extraction technique. *Weld World* 59:137–144. <https://doi.org/10.1007/s40194-014-0186-z>
- DIN EN ISO 9015-1 (2011) Destructive tests on welds in metallic materials - Hardness testing - part 1: hardness test on arc welded joints. German version of EN ISO 9015-1. Beuth-Verlag, Berlin, Germany. <https://doi.org/10.31030/1751808>
- Ortner B (1985) The choice of lattice planes in X-ray strain measurements of single crystals. *Adv X Ray Anal* 29:113–118. <https://doi.org/10.1154/S0376030800010181>
- Ortner B (1985) Simultaneous determination of the lattice constant and elastic strain in cubic single crystal. *Adv X Ray Anal* 29:387–394. <https://doi.org/10.1154/S0376030800010491>
- Winholtz RA, Cohen JB (1988) Generalised least-squares determination of triaxial stress states by X-ray diffraction and the associated errors. *Aust J Phys* 41(2):189–199
- Mente T, Boellinghaus T, Schmitz-Niederer M (2012) Heat treatment effects on the reduction of hydrogen in multi-layer

- high-strength weld joints. *Weld World* 56(7/8):26–36. <https://doi.org/10.1007/BF03321362>
27. Boellinghaus T, Mente T, Wongpanya P et al (2016) Numerical modelling of hydrogen assisted cracking in steel welds. In: Boellinghaus T, Cross C (eds) *Cracking phenomena in welds IV*. Springer, Cham (Switzerland)
  28. Richter F (1991) *Die physikalischen Eigenschaften der Stähle - Das 100 Stähle Programm. Teil I: Tafeln und Bilder*. [https://www.tugraz.at/fileadmin/user\\_upload/Institute/IEP/Thermophysics\\_Group/Files/Staehle-Richter.pdf](https://www.tugraz.at/fileadmin/user_upload/Institute/IEP/Thermophysics_Group/Files/Staehle-Richter.pdf). Accessed 18 August 2023
  29. Boellinghaus T, Hoffmeister H, Dangeleit A (1995) A scatterband for hydrogen diffusion coefficients in micro-alloyed and low carbon structural steels. *Weld World* 35(2):83–96
  30. Rhode M, Nietzke J, Mente T et al (2022) Characterization of hydrogen diffusion in offshore steel S420G2+M multi-layer submerged arc welded joint. *J Mater Eng Perf* 31:7018–7030. <https://doi.org/10.1007/s11665-022-06679-7>
  31. Mente T, Boellinghaus T (2012) Modeling of hydrogen distribution in a duplex stainless steel. *Weld WorldActa Mater* 56:66–78. <https://doi.org/10.1007/BF03321397>
  32. DIN EN IO 5817 (2023) *Welding - fusion-welded joints in steel, nickel, titanium and their alloys (beam welding excluded) - quality levels for imperfections. German version EN ISO 5817*. Beuth-Verlag, Berlin, Germany. <https://doi.org/10.31030/3428947>
  33. Tasak E, Ziewiec A, Adamiec JA (2011) The role of hydrogen in weld cracking processes - a new look at the problem. *Weld Int* 25(6):409–414. <https://doi.org/10.1080/09507111003655200>
  34. Heinze C (2014) *Untersuchung der Mikrorissbildung beim Schweißen hochfester Feinkornbaustähle*. Dissertation (in German). Technische Universität, Berlin, Germany
  35. Wilhelm E, Mente T, Rhode M (2021) Waiting time before NDT of welded offshore steel grades under consideration of delayed hydrogen-assisted cracking. *Weld World* 65:947–959. <https://doi.org/10.1007/s40194-020-01060-5>

**Publisher's note** Springer Nature remains neutral with regard to jurisdictional claims in published maps and institutional affiliations.